Observing with ASKAP: Optimisation for survey speed

D McConnell
CSIRO Astronomy and Space Science
ACES memorandum 015

3rd October 2017

1 Introduction

The survey speed and uniformity of sensitivity over an area imaged by ASKAP are influenced by the parameter values chosed for the observation. Survey speed depends on familiar parameters such as collecting area, bandwidth and integration time, but also on the PAF field-of-view and the arrangement of beams within it. A full estimation of likely survey speed relies on measurements of performance. Now, with a partially equipped array, the performance measurements are becoming complete enough to attempt some realistic forecasts.

The subject of this note is the generation of such forecasts and the impact of the choice of particular observing parameters: the number, spacing and arrangement of the formed beams. The forecasts presented here can be compared with estimates made from theoretical models of phased array feeds reported by Bunton & Hay (2010).

2 Survey speed

Johnston et al. (2007) give an expression for survey speed for an interferometer with N antennas of area A observing over bandwidth B. The expression gives the area of sky that can be surveyed in one second to a depth equivalent to image noise of σ_s:

$$\mathrm{SS}_s = FBn_p \left(\frac{AN\epsilon_a\epsilon_c\sigma_s}{2kT} \right)^2 \tag{1}$$

Here n_p is the number of polarizations, ϵ_a and ϵ_c are aperture and correlator efficiencies, T is the system temperature and k is Boltzmann's constant. F is the field of view. The expression for SS_s can be rewritten in terms of the measurable quantity SEFD (System Equivalent Flux Density):

$$\mathrm{SEFD} = \frac{2kT}{A\epsilon_a\epsilon_c} \tag{2}$$

so

$$\mathrm{SS}_s = FBn_pN^2\sigma_s^2 w \tag{3}$$

where

$$w = \frac{1}{\mathrm{SEFD}^2} \tag{4}$$

We measure the SEFD at beam centres, but the effective SEFD over a beam varies inversely with the relative beam gain. Thus, correcting an image for the beam attenuation off-axis increases the image noise away from beam centre. Let SEFD_0 be the measured quantity, then in the image corrected for beam attenuation:

$$\mathrm{SEFD}(l,m) = \frac{\mathrm{SEFD}_0}{\mathcal{A}(l,m)} \tag{5}$$

where $\mathcal{A}(l,m)$ is the normalised antenna (or beam) power pattern. Recognising that SEFD (and so w) varies over the field of view, write the survey speed expression as:

$$\mathrm{SS}_s = Bn_pN^2\sigma_s^2 \int\int_{FoV} w(l,m)\, dl\, dm \tag{6}$$

where l, m are direction cosines and the integral is over the PAF angular field-of-view. Recent measurements allow us to estimate $w(l,m)$.

3 Uniformity of survey sensitivity

The survey speed expression relates to the integral of sensitivity, independent of the varition of sensitivity over the field of view. If w has large variablity with (l,m), a more uniform sensitivity can be achieved by dividing the observing time between a number of pointings with no loss of total survey speed. This shifting of pointing position is referred to as interleaving. ASKAP forms up to 36 beams within its field-of-view. The best interleaving strategy will depend on both the arrangement of beams (the footprint) and the form of the overall envelope of sensitivity across the field of view. The

recent measurements allow some estimation of this sensitivity envelope—the apodizing function—to be made.

Interleaving can be done by cycling the telescope pointing between the several centres during the course of a single synthesis observation, with some loss of integration time to the associated overheads. Alternately, if the total integration time required is sufficient, the different interleaving points can be observed uninterrupted for separate observations.

4 Beam-to-beam correlation

Beams are formed as the weighted sum of signals from PAF elements. In general, any two beams will have some PAF elements in common so that their signals are not completely independent. The degree of correlation between them rises with decreasing angular separation. As a consequence, the linear mosaic of images made from a set of PAF beams will have more image noise than would be achieved from a set of images with independent noise. An estimate of the correlation coefficient as a function of beam separation is given here (see ACES memorandum 014 for details.)

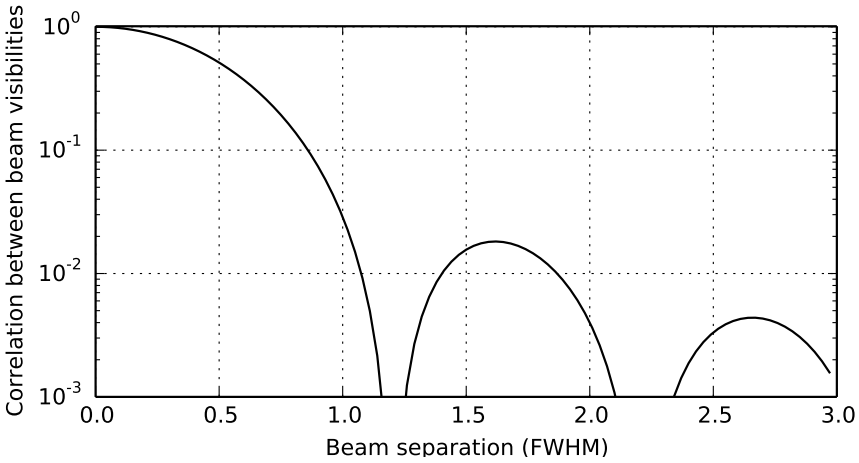

Figure 1: The modelled correlation coefficient between visibilities for two beams as a function of their separation. Beam weights for each PAF element are assumed to be proportional to the amplitude of the signal received by that element. The model is constructed from an idealised 2-dimensional Airy voltage pattern.

The Figure 2 below illustrates the limiting effect of the correlation. When images are formed from independent observations, so that the noise in each beam is mutually independent, the linear mosaic has improved sensitivity in the region of overlap as shown in the left hand panel; each curve shows a different spacing of beams. The total survey speed achieved is proportional to the integral under the curves, which is invariant with beam spacing. On the right, once the beam-to-beam correlation is included, there is significant penalty in arranging beams too closely: the integral decreases with beam separation.

The sensitivity in the PAF field-of-view can nowhere exceed that in the centre of a single beam.

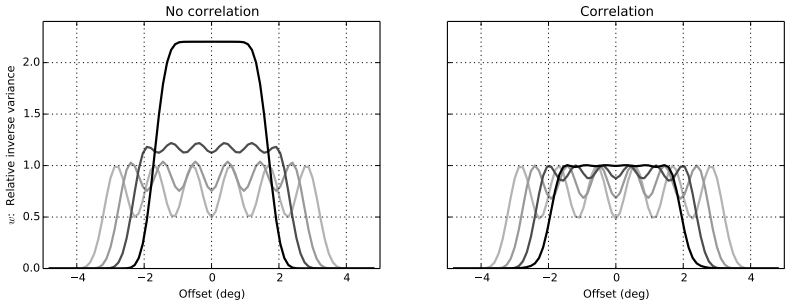

Figure 2: Observation weight for different beam spacings with no beam-to-beam correlation (left) and with the expected correlation (right). The quantity plotted is the profile of inverse-variance, relative to the inverse variance of a single bore-sight beam, over a set of six evenly spaced beams. The four traces correspond to beam spacings 0.5 (dark), 0.7, 0.85 and 1.0 (light) times the beam FWHM.

5 Measured apodizing function

The sensitivity of ASKAP beams is expected to fall with increasing angular distance from the boresight. A large part of this decrease is due to increasingly large parts of the antenna's diffraction pattern on the focal plane moving off the sensitive portion of the PAF as the beams' angular displacement increases. For this analysis we model the system with a set of beams of identical sensitivity that are attenuated by an "apodizing" function, the sensitivity envelope that defines the PAF field-of-view. The form of the

apodizing function was established as follows. Measurements of SEFD were made for each beam in four different footprints, the 6×6 square and hexagonal footprints (`square_6x6`, `hexagon36`) at position angles 0 and 45 degrees. For each footprint the relative sensitivity for each beam i was calculated as $\mathrm{SEFD}_{min}/\mathrm{SEFD}_i$. Values of the SEFD were calculated for each of the 12 antennas for each beam over the frequency range 1376.5 - 1424.5 MHz. The spectral median was used for SEFD_i. A relative sensitivity surface was determined for each antenna by gridding the data onto a regular grid over the field-of-view. The mean surface over 11 antennas (AK13 produced anomalous results for several of the observations) was adopted as a representative measure of the apodizing function, and is shown at left in Figure 3. To provide an analytic apodizing function for the survey-speed calculations in this memo, the measured surface was fit to a family of functions, symmetric about the centre of the field.

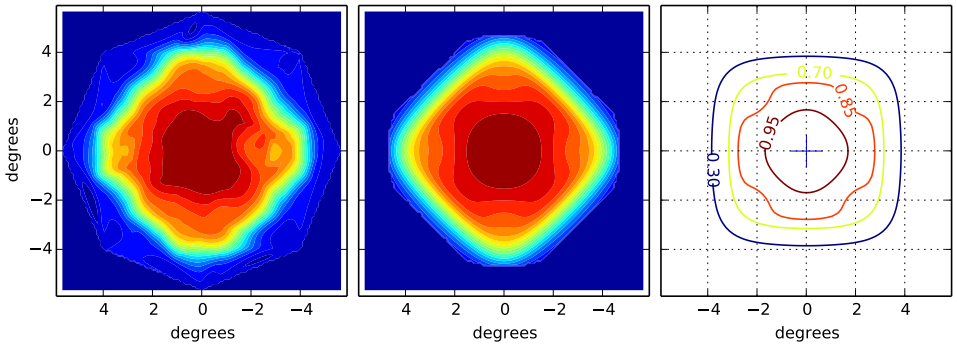

Figure 3: Left: Measured estimate of the relative sensitivity envelope—the apodizing function—over the PAF field-of-view; coloured contours lie in even steps from 0.05 to 0.95. Centre: Best-fit model to the measurement on the left; the functions used in the model are constrained to be symmetric. Right: Envelope model rotated 45 degrees.

The quasi-rectangular footprints in general use are usually aligned with celestial coordinates, and so at 45 degrees to the natural orientation of the field-of-view. A better fit, and therefore survey speed, is achieved with either the footprint or the PAF rotated 45 degrees. In this memo we have assumed that the PAF is rotated for observations, so that the function in the right hand panel of Figure 3 is used for sensitivity calculations.

6 Variation of survey speed with beam pitch

For a given footprint, the value of $\bar{w} = \int \int_{FoV} w(l,m)\, dl\, dm$ varies with beam separation. Because the beam-to-beam correlation limits the sensitivity of mosaiced overlapping beams (see Figure 2), the value of $\bar{w}$ increases with increasing pitch up to a certain level. Beyond that pitch, $\bar{w}$ decreases because the outer beams become attenuated by the apodizing function. Figure 4 illustrates this.

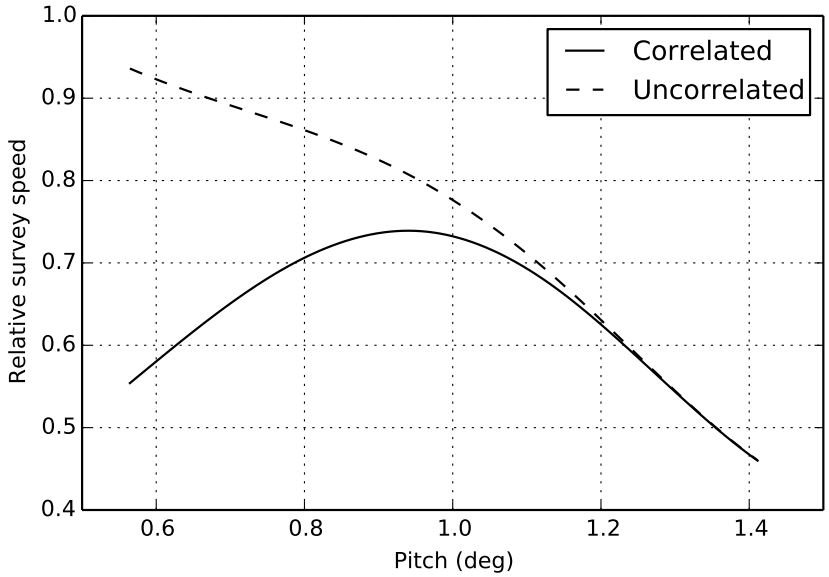

Figure 4: Variation of $\bar{w}$ with beam pitch, relative to the value obtained from the fictitious case of no attenuation from an apodizing envelope and no beam-to-beam noise correlation. The dashed line shows the effect of a realistic apodizing but with no beam-to-beam correlation. The solid line includes the effect of correlation between beams. The survey speed obtained from both the correlated and uncorrelated footprints declines as the beams move to the outer parts of the field-of-view. For the realistic case with correlated noise, sensitivity improves as the beam overlap decreases until the edge of the PAF field-of-view is reached. For this simulation a square 6×6 footprint was used with model ASKAP 1.4GHz beams.

7 Beam footprints and interleaving schemes

In the following sections we model performance for a number of specific beam footprints. Each has its own natural interleaving scheme depending on its geometry. The aim of interleaving is to have a sequence of pointings that place beam centres in the sensitivity depressions of the previous pointing in the sequence. The square footprints (`square_6x6`, `square_5x5`) have one depression for each beam so a pair of pointings can produce a square grid with spacing $1/\sqrt{2}$ times the spacing of the single footprint. The footprints with hexagonal geometry (`closepack36`, `closepack30`) have two depressions per beam, so a set of three pointings is necessary to form a new uniform hexagonal grid, which has beam spacing $1/\sqrt{3}$ times the spacing of the single footprint.

The special rectangular footprint invented by Josh Marvil, `rectangle_6x6`, has beams on a rectangular grid with beam pitches p and $p\sqrt{3}/2$. With three additional pointings a hexagonal grid can be formed with final beam spacing $p/2$.

Figure 5 shows the three types of beam grids.

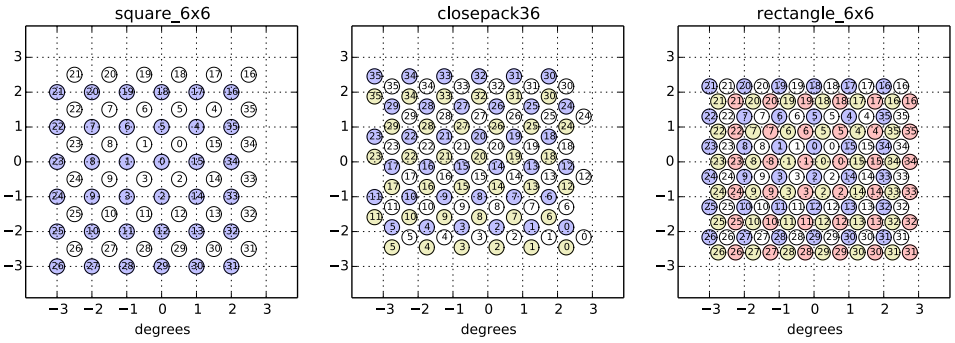

Figure 5: Three interleaved footprints: `square_6x6` (left), `closepack36` (middle) and `rectangle_6x6` (right), requiring two, three and four interleaved pointings respectively. Each beam is numbered, and coloured according its pointing, in order white, blue, yellow, red. All three footprints displayed were constructed with beam pitch $p = 1.0°$.

8 Optimising at selected frequencies

Using the assumed apodizing function and the beam-to-beam correlation model, for a given footprint and observing frequency we can estimate the beam pitch that gives the highest survey speed. From the model we can determine the equivalent area of the observation and the residual ripple, before and after interleaving. These quantities are given in Figure 6.

Some points to be noted:

- The smaller footprints (those with fewer beams) tolerate a larger pitch.
- The survey speed is maximised by using all 36 beams, independent of arrangement and frequency.
- For the 36-beam footprints, frequency is the main determinant of equivalent area.
- Even for the square footprints, the sensitivity ripple after interleaving (e.g. 1% at 1400 MHz with `square_6x6`) is much less than the sensitivity variation across the field-of-view from the apodizing function.
- The results here are critically influenced by the form of the apodizing function. More work is needed to estimate the level of uncertainty in the current model.

Figure 7 shows how critically survey speed depends on beam pitch.

9 Nyquist sampling the sky

To be maximally sensitive to very extended sky emission, the spacing of beam positions across the imaged region should satisfy the Nyquist sampling criterion (Cornwell 1988). The MIRIAD manual gives this criterion for both square and hexagonal grids of beam placement. The spacings corresponding to the Nyquist sampling limit are:

$$\begin{aligned} \theta_{\rm squ} &= \frac{\lambda}{2D} \\ \theta_{\rm hex} &= \frac{2}{\sqrt{3}}\frac{\lambda}{2D} \end{aligned} \tag{7}$$

Figure 8 plots the ratio of post-interleaving beam spacing for square and hexagonal footprints to their respective sampling limits. After mosaicing the interleaved pointings, the beam spacings, for pitch p are $\frac{p}{\sqrt{2}}$ and $\frac{p}{\sqrt{3}}$ for square and hexagonal footprints respectively. After the four pointings needed to interleave the rectangular footprint the beam spacing is $p/2$.

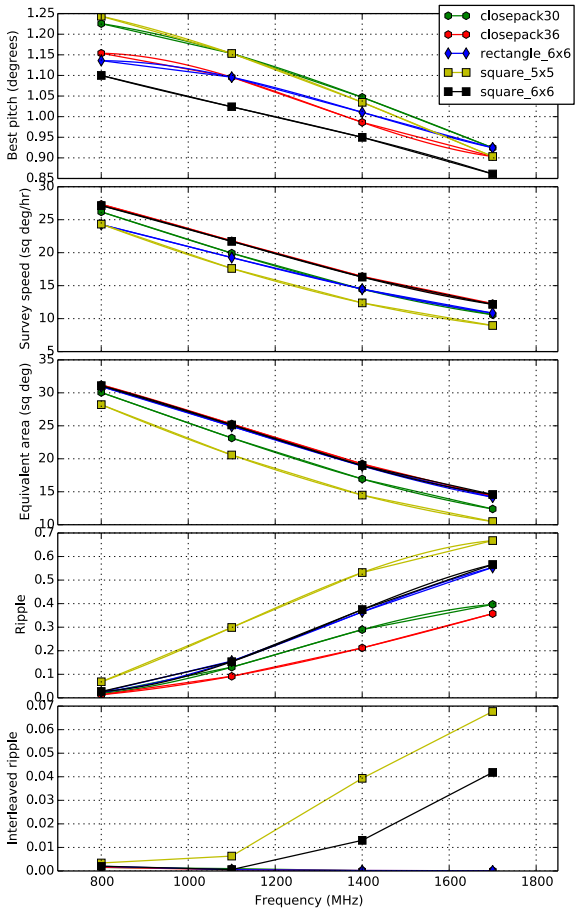

Figure 6: From top to bottom the plots show as a function of frequency: the beam pitch that optimises survey speed; the optimised survey speed; the equivalent area; the ripple of the optimised footprint before and after interleaving. The model was evaluated at the four indicated frequencies; a smooth curve joins the calculated values. The ripple is computed as (max-min)/mean over a portion of the centre of the mosaiced field. The equivalent area of the single observation (not interleaved) is shown and is calculated as $\frac{\int\int_{FoV} w(l,m)\, dl\, dm}{w_{\max}}$. The survey speed values were computed using $\mathrm{SEFD}_0 =$ 1900Jy in equation 5, and equation 6 with $B = 300$MHz, $n_p = 2$, $N = 12$ and $\sigma_s = 100\mu$Jy.

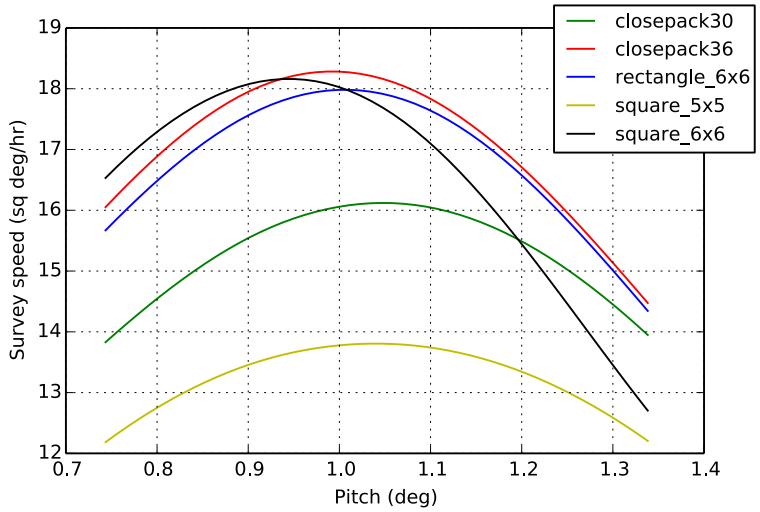

Figure 7: Dependence of survey speed on beam pitch for the set of footprints. The survey speed values were computed using equation 6 with $B = 300$MHz, $n_p = 2$, $N = 12$ and $\sigma_s = 100\mu$Jy.

10 Footprint displays

The following figures show the footprint at their optimum pitch. There are three panels for each footprint-frequency combination. They show: Left: beam position relative to the assumed apodizing function $1/\sqrt{2}$ contour; Centre: sensitivity map of a single non-interleaved observation; Right: sensitivity map of the mosaiced interleaved observations.

References

Bunton, J. D., & Hay, S. G. 2010, Electromagnetics in Advanced ...
Cornwell, T. J. 1988, AA, 202, 316
Johnston, S. et al. 2007, PASA, 24, 174

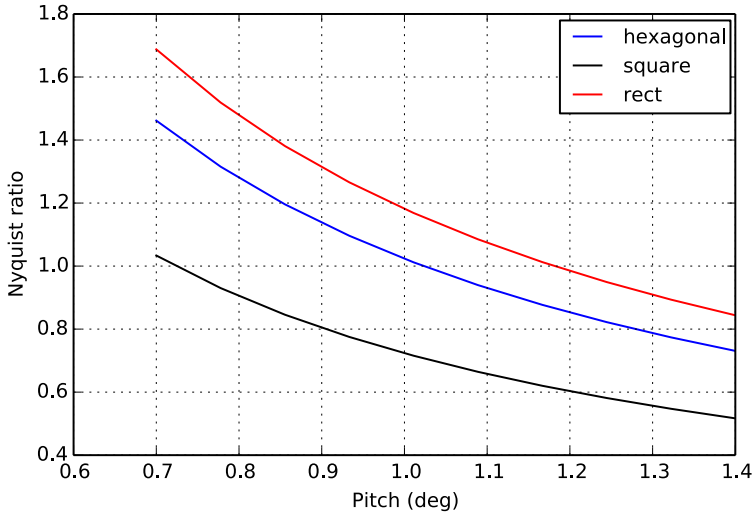

Figure 8: Ratio of beam spacing to the Nyquist sampling limit: $\frac{\lambda}{2D}$ and $\frac{2}{\sqrt{3}}\frac{\lambda}{2D}$ for square and hexagonal footprints, respectively, calculated for frequency $f = 1400$MHz. The rectangular footprint results in a hexagonal grid after interleaving, so the latter factor is used for it. The beam spacing used is that of the mosaic of all interleaved pointings.

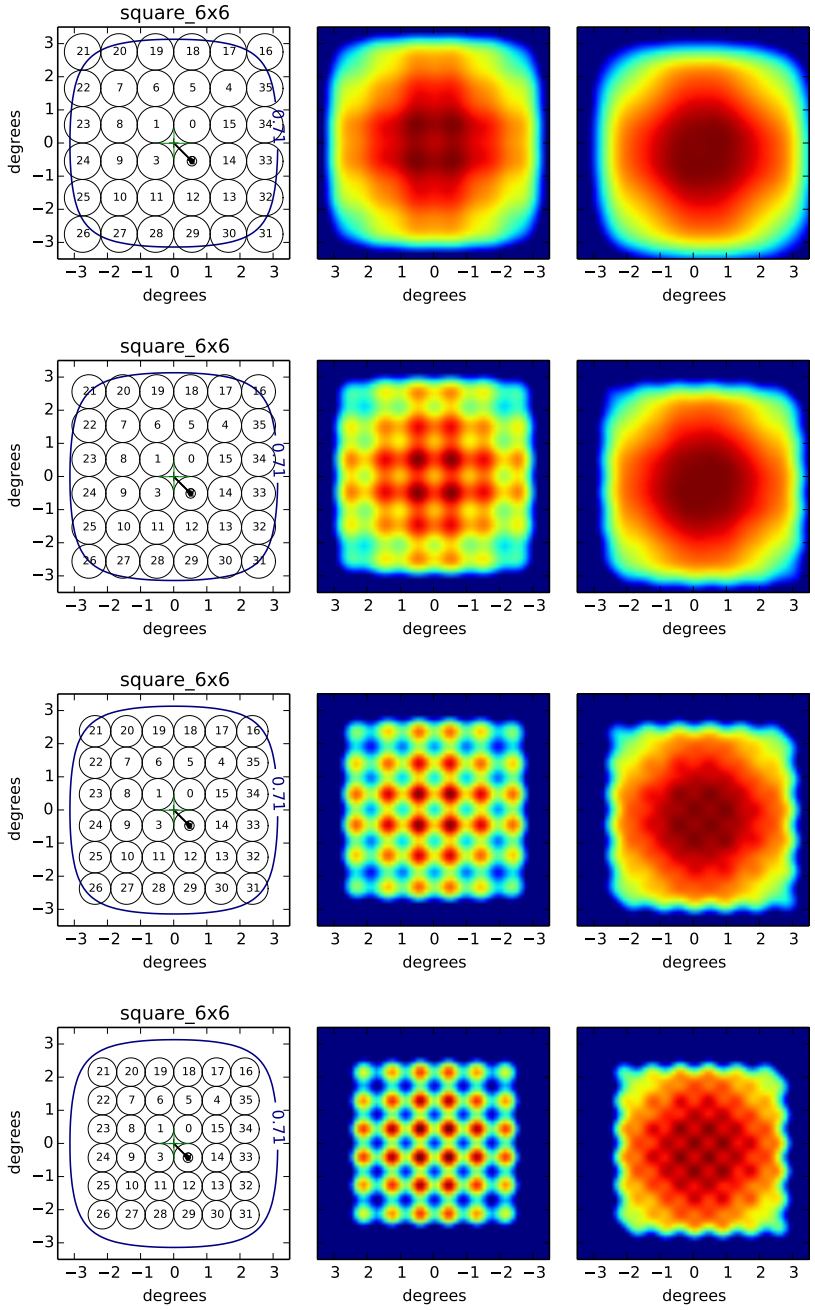

Figure 9: Footprint `square_6x6` at 800, 1100, 1400, 1700 MHz (top to bottom).

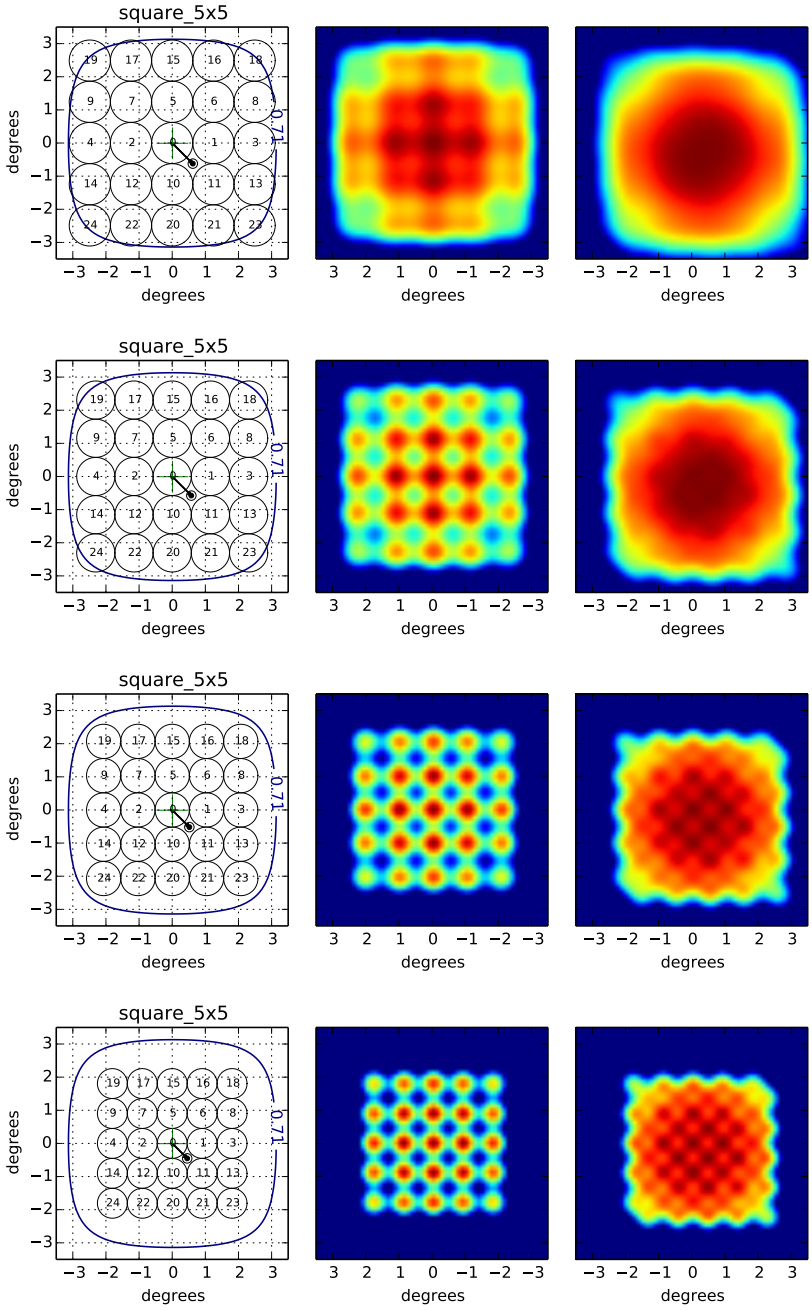

Figure 10: Footprint `square_5x5` at 800, 1100, 1400, 1700 MHz (top to bottom).

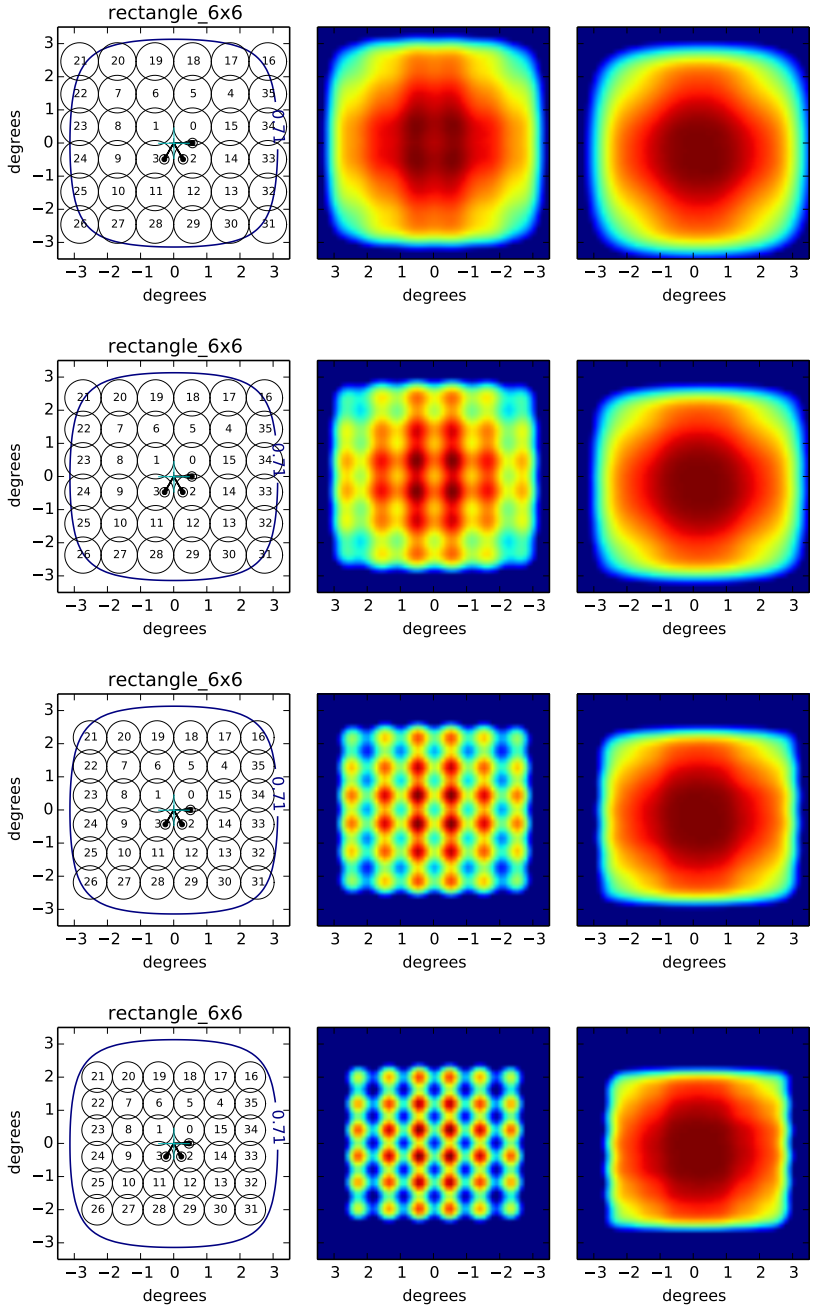

Figure 11: Footprint `rectangle_6x6` at 800, 1100, 1400, 1700 MHz (top to bottom).

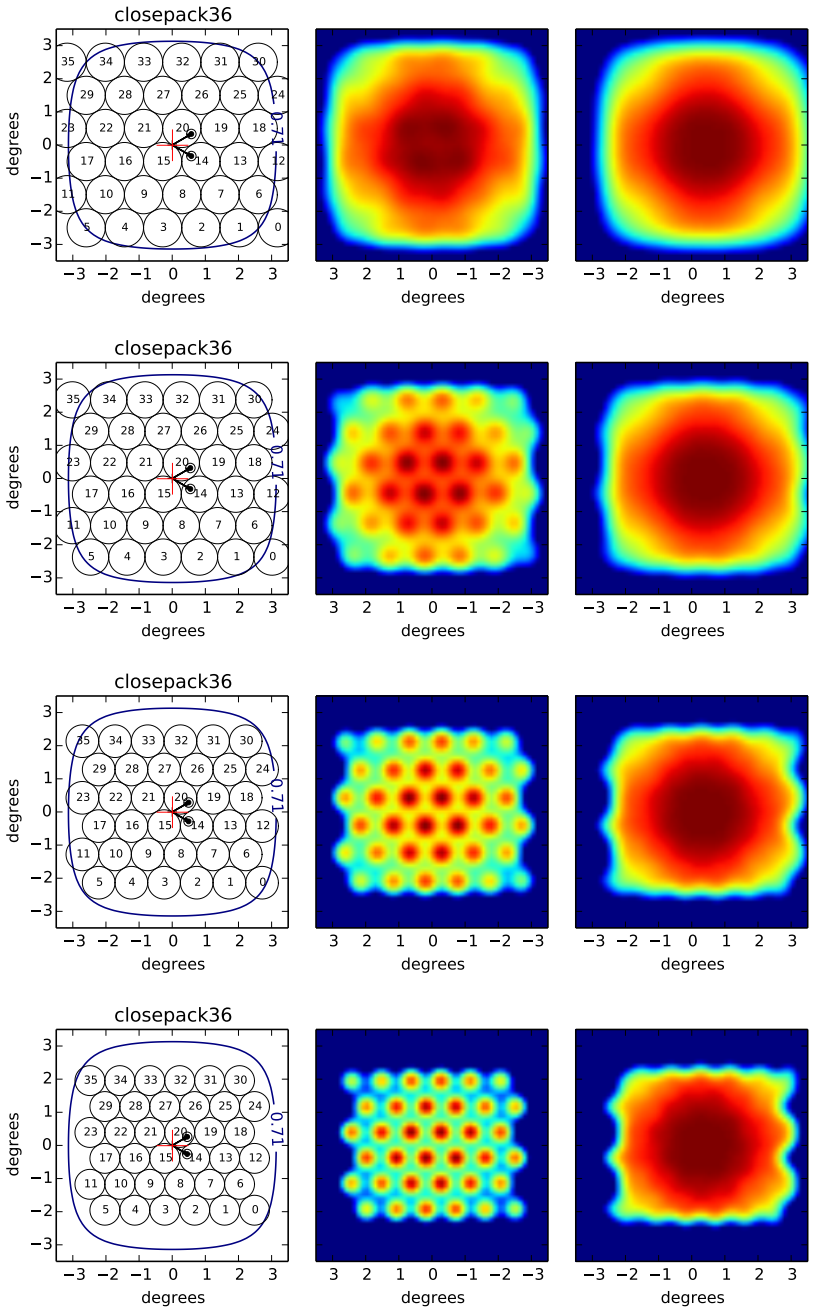

Figure 12: Footprint `closepack36` at 800, 1100, 1400, 1700 MHz (top to bottom).

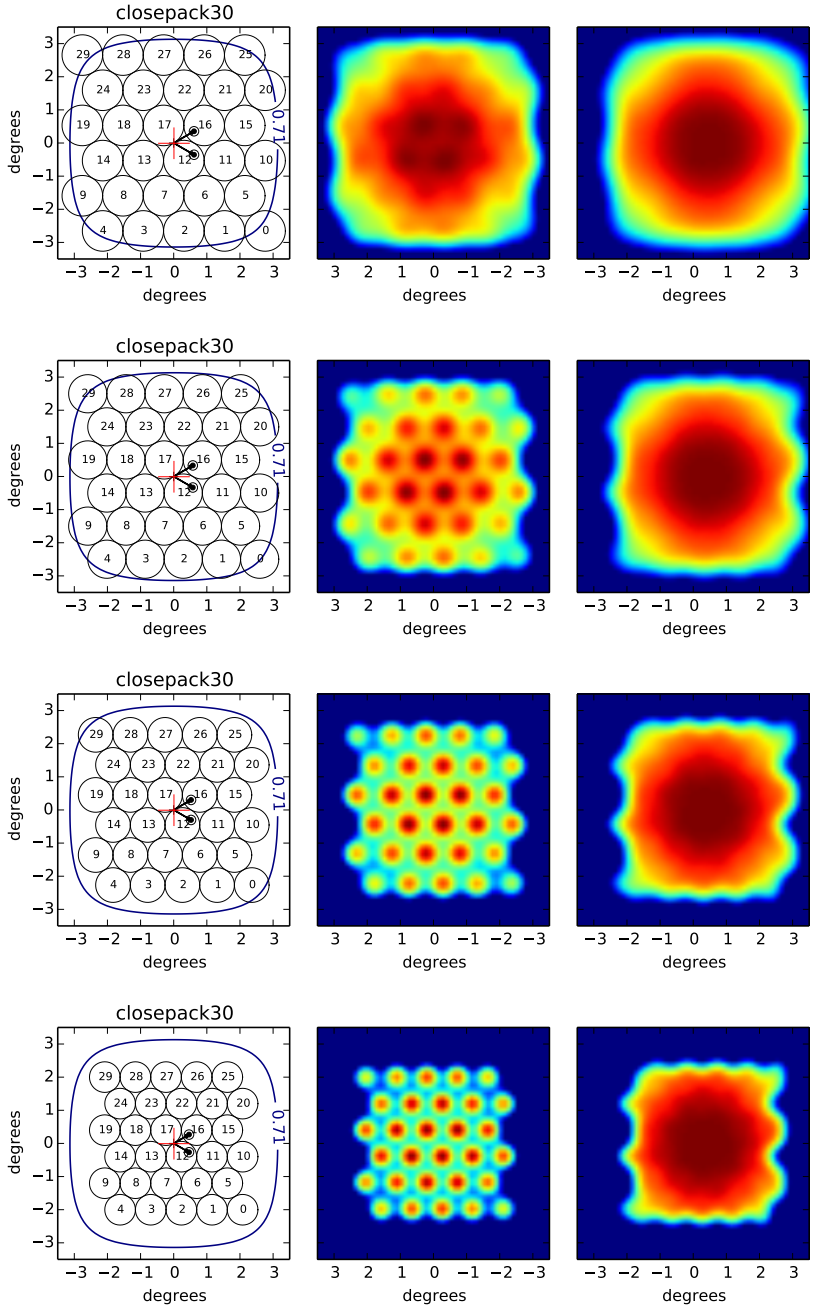

Figure 13: Footprint `closepack30` at 800, 1100, 1400, 1700 MHz (top to bottom).